Supplemental Material:

1. Optical images of CVD grown MoS_2 on SiO_2/Si with different magnifications as shown in (a) (b), and Raman spectra showing both photoluminescence peaks and Raman peaks of single-layer and double-layer MoS_2 grown on SiO_2/Si in (c) (d).

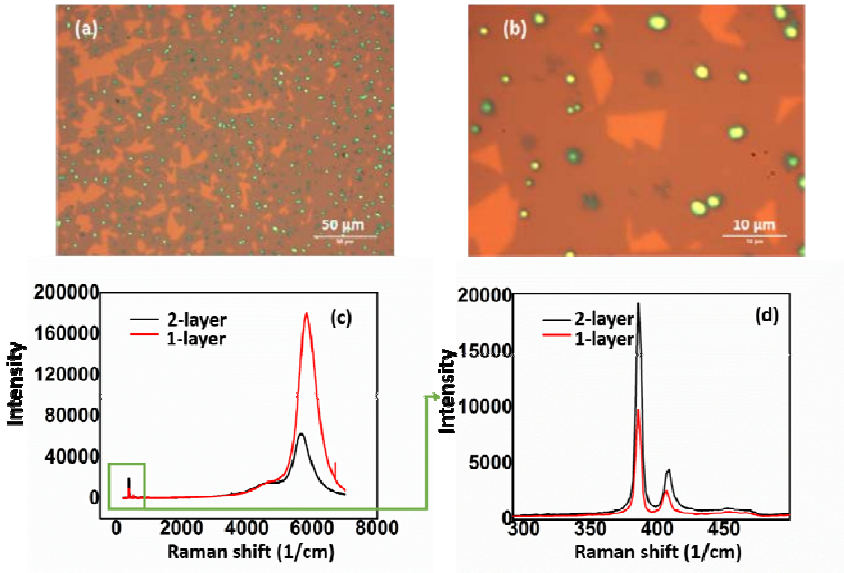

2. Raw large-area ADF images of single-layer MoS_2 (a), boundary between single-layer and bi-layer MoS_2 (b), and boundary between bi-layer and tri-layer MoS_2 (c).

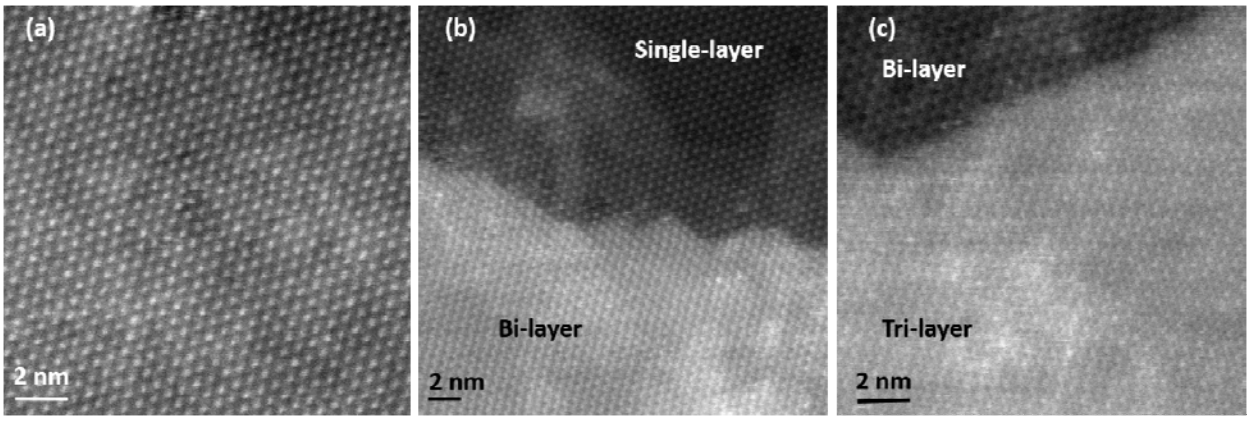

3. ADF image (raw) of one type of bi-layer MoS_2 with a certain relative rotation angle. The relative rotation angle between layers is measured to be around 6° from FFT shown in the inset of the figure.

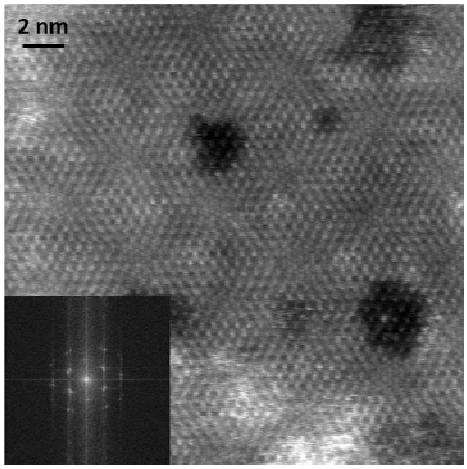

4. Simulated images of tri-layer MoS_2 with the first two layers stacked as AA' ((a) to (d)), plus 3R phase (e) which has the stacking sequence (AB)B. Simulation of these ADF images is based on multi-slice theory. For the simulation, we use 50keV as the energy for the electron source, 32 mrad as the convergence semi-angle (probe size approximately 1.7 Å), and 77-385 mrad as the collection semi-angles, which all match the experimental conditions. Spherical aberration Cs is set to be 0 (to simulate the aberration-corrected probe) and the simulation sampling is 0.05 Å/pixel. The probe defocus is kept at 0, with a probe spacing of 0.11 Å. We divide the unit cell into 4 slices for single-layer case, 8 slices for bi-layer and 12 slices for tri-layer. We use 16 frozen phonon configurations for all simulations to account for thermal vibration.

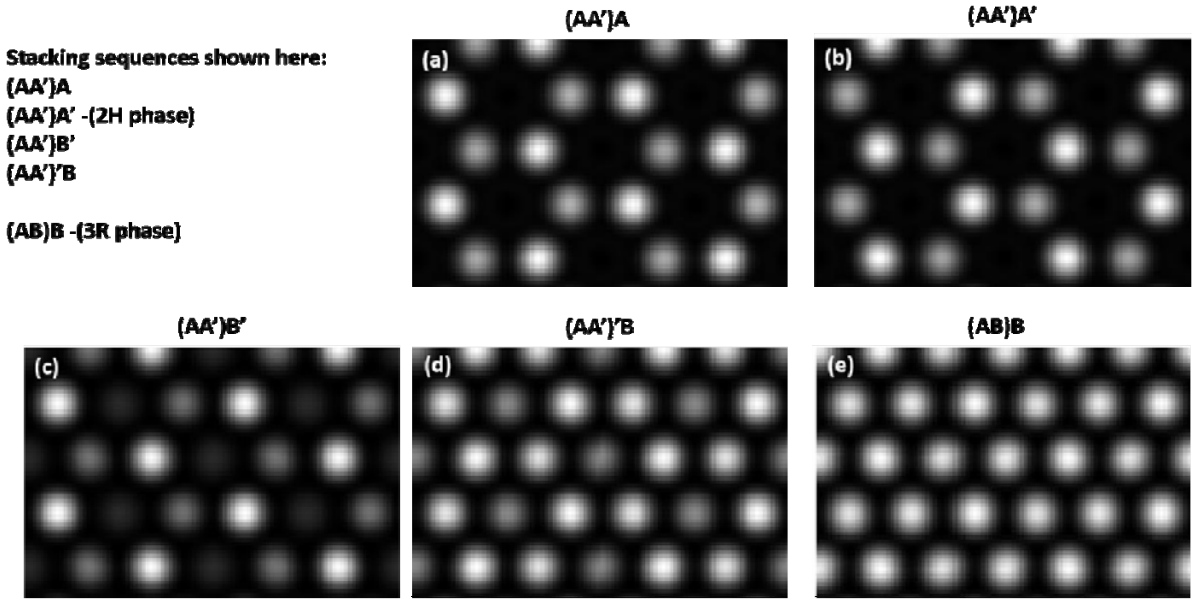

5. ADF images of tri-layer MoS_2 with the stacking sequence AA'B from different patches of growth. Low-pass filter was applied to both images.

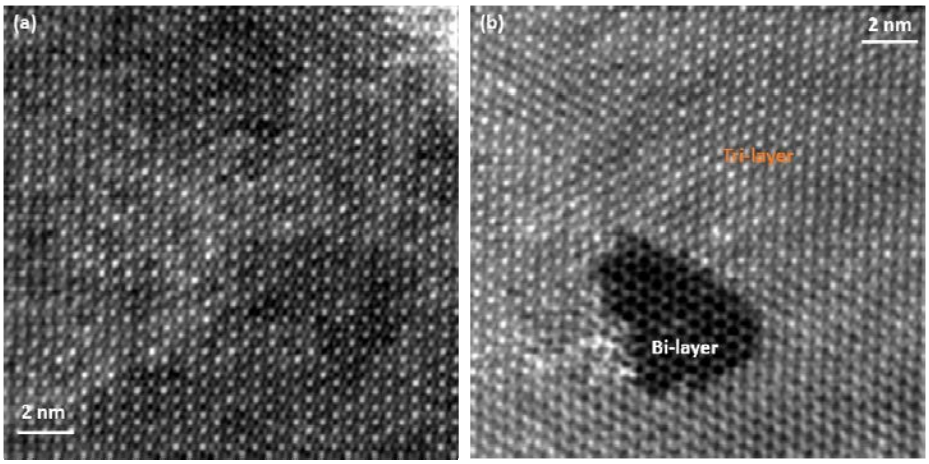

6. DFT simulation of the total energies of all possible stacking sequences in bi-layer (table 1) and tri-layer MoS_2 (table 2).

Table 1:

Bi-layer MoS_2	
Stacking Sequence	Total energy(eV)/unit cell
AA'	-44.7419
AB	-44.7416
AB'	-44.7290
A'B	-44.6889
AA	-44.6859

Table 2:

Tri-layer MoS_2		
Stacking Sequence	Equivalent stacking	Total energy (eV)/unit cell
(AA')A'	(AA')A'	-67.1968
(AA')B	(AB)A'	-67.1963
(AB)B	(AB)B	-67.1960
(AA')B'	(AB')A'	-67.1840
(AB)B'	(AB')B	-67.1839
(AB')B'	(AB')B'	-67.1712
(AA')'B	(A'B)A'	-67.1428
(AB)'A	(A'B)B	-67.1423
(AA)B	(AB)A	-67.1397
(AA)A'	(AA')A	-67.1396
(AB')'B	(A'B)B'	-67.1301
(AA)B'	(AB')A	-67.1276
(A'B)'B	(A'B)'B	-67.0887
(AA)'B	(A'B)A	-67.0863
(AA)A	(AA)A	-67.0838